

## NUMERICAL INVESTIGATION ON THE PERFORMANCE OF COALESCENCE AND BREAK-UP KERNELS IN SUBCOOLED BOILING FLOWS IN VERTICAL CHANNELS

Sara VAHAJI<sup>1</sup>, Lilunnahar DEJU<sup>1</sup>, Sherman C.P. CHEUNG<sup>1</sup>, Guan YEOH<sup>2,3</sup> and Jiyuan TU<sup>1\*</sup>

<sup>1</sup> School of Aerospace, Mechanical and Manufacturing Engineering (SAMME), RMIT University, Victoria 3083, Australia

<sup>2</sup> Australian Nuclear Science and Technology Organisation (ANSTO), Locked Bag 2001, Kirrawee DC, NSW 2232, Australia

<sup>3</sup> School of Mechanical and Manufacturing Engineering, University of New South Wales, Sydney, NSW 2052, Australia

\*Corresponding author, E-mail address: Jiyuan.tu@rmit.edu.au

### ABSTRACT

In order to accurately predict the thermal hydraulic of two-phase gas-liquid flows with heat and mass transfer, special numerical considerations are required to capture the underlying physics: characteristics of the heat transfer and bubble dynamics taking place near the heated wall and the evolution of the bubble size distribution caused by the coalescence, break-up and condensation processes in the bulk subcooled liquid. The evolution of the bubble size distribution is largely driven by the bubble coalescence and break-up mechanisms. In this paper, a numerical assessment on the performance of six different bubble coalescence and break-up kernels is carried out to investigate the bubble size distribution and its impact on local hydrodynamics. The resultant bubble size distributions are compared to achieve a better insight of the prediction mechanisms. Also, the void fraction, mean Sauter bubble diameter, and interfacial area concentration profiles are compared against the experimental data to ensure the validity of the simulations.

**Keywords:** Population balance; coalescence; break-up; multiphase heat and mass transfer; subcooled boiling flow; wall heat partitioning

### NOMENCLATURE

$a$	coalescence rate
$a(M_i, M_j)$	coalescence rate of $i$ and $j$ bubble class in terms of mass
$a_{if}$	interfacial area concentration
$B_B, B_C$	mass birth rate due to break-up and coalescence
$C_1, C_2, C_3, C_{C&T}$	coalescence model constant
$C_D$	drag coefficient
$C_L$	lift coefficient
$C_{MB}, K_g$	breakage model constant
$d_{ij}$	equivalent diameter
$D_S$	mean Sauter bubble diameter
$D_B, D_C$	mass birth rate due to break-up and coalescence
$e(\lambda)$	kinetic energy of eddy with size $\lambda$
$E_o$	Eötvös number
$E_{o_d}$	modified Eötvös number
$f$	size fraction
$f_{BV}$	break-up volume fraction, $v_i/v_j$
$F_{lg}^{drag}$	drag force

$F_{lg}^{lift}$	lift force
$F_{lg}^{wall\ lubrication}$	wall lubrication force
$F_{lg}^{turbulent\ dispersic}$	turbulent dispersion force
$h$	Inter-phase heat transfer coefficient
$h_o$	initial film thickness
$h_f$	critical film thickness
$h(M_i, M_j)$	collision frequency in terms of mass
$M$	mass scale of gas phase (bubble)
$n$	average bubble number density or weight
$P$	pressure
$P_b$	breakage probability
$P_e(e(\lambda))$	energy distribution function
$r$	breakage rate
$r(M_i, M_j)$	partial breakage rate in terms of mass for $i$ bubble class breaking into $j$ and $(i-j)$ bubble class
$r(M_i)$	total breakage rate of $i$ bubble class in terms of mass
$S_i$	mass transfer rate due to coalescence and break-up
$t$	physical time
$t_{ij}$	time for two bubbles to coalesce
$T_{sub}$	subcooling temperature
$\mathbf{u}$	velocity vector
$u_t$	turbulent velocity
$V$	volume of bubble
Greek symbols	
$\alpha$	void fraction
$\alpha_{max}$	maximum allowable void fraction
$\beta(f_{BV}, 1)$	daughter bubble size distribution
$\varepsilon$	dissipation of turbulent kinetic energy
$\eta_{kli}$	coalescence mass matrix
$\lambda$	size of eddy in inertial sub-range
$\lambda(M_i, M_j)$	coalescence efficiency in terms of mass
$\lambda_{min}$	minimum size of eddy in inertia sub-range defined as $11.3(v^3/\varepsilon)^{1/4}$
$\mu$	viscosity
$\rho$	density
$\sigma$	surface tension
$\tau_{ij}$	contact time for two bubbles
$\xi$	internal space vector of the PBE or size ratio between an eddy and a particle
$\Gamma$	interfacial mass transfer rate
Super/Subscripts	
$e$	effective
$i, j, k$	index of gas bubble class
$t$	turbulent
$g$	gas phase
$l$	liquid phase

## INTRODUCTION

Two-phase gas-liquid flows with heat and mass transfer, such as subcooled boiling flows in heated channels, are prevalent in various industrial applications. In order to accurately predict the thermal hydraulic of such flows, special numerical considerations are required to capture the underlying physics: characteristics of the heat transfer and bubble dynamics taking place near the heated wall and the evolution of the bubble size distribution caused by the coalescence, break-up and condensation processes in the bulk subcooled liquid. It is well known that the evolution of the bubble size distribution is largely driven by the bubble coalescence and break-up mechanisms. A number of mechanistic coalescence and break-up kernels have been proposed in the past decades. Nevertheless, the performance of these kernels in subcooled boiling flows remains elusive.

The Eulerian-Eulerian approach - two-fluid model - is a promising tool to capture the local hydrodynamics. Most of the interfacial force models need a closure of bubble size distribution or the interfacial area concentration. Some studies assumed a single bubble size to tackle the problem. However, this assumption introduces inaccuracies into the numerical modelling. Hence, Population Balance Modelling has emerged to model the bubble coalescence and break-up to capture the bubble dynamics. One of the promising approaches in population balance modelling is the Multiple Sized Group (MUSIG) model, in which in addition to the continuity equation, bubbles are discretised into a series of bubble size classes. The bubble changes due to coalescence and break-up are accommodated by a scalar equation for each bubble size class.

Over the past decades, the coalescence and break-up phenomenon have been investigated extensively in both experimental and theoretical fields. A comprehensive study on these models is done by Liao and Lucas (2009), and Liao and Lucas (2010). Although a variety of models are available, one has to investigate their performance and applicability. Only a few studies have been carried out to evaluate the performance of a range of coalescence and breakage kernels in two-phase flow. Recently, Deju *et al.* (2015) carried out a comparative analysis of different coalescence and break-up kernels in a large bubble column; however, such investigations on subcooled boiling flows remain elusive.

The heat transfer mechanisms happening at the heated wall and influencing on the bubble dynamics are considered through the wall heat partitioning model through a mechanistic approach and explained in our previous work (Yeoh *et al.* (2014)).

Hence, the main focus of this work is to gain more insight on the applicability of existing models in capturing the bubble coalescence and breakage phenomenon in subcooled boiling flows with different experimental conditions. In this paper, a numerical assessment on the performance of six different bubble coalescence and break-up kernels is therefore carried out to investigate the bubble size distribution and its impact on local hydrodynamics. For the break-up kernels, two widely adopted models with different predictions for daughter size distribution (DSD) proposed by Luo and Svendsen (1996) and Wang *et al.* (2003) are selected. These break-up kernels are then coupled with three different coalescence kernels by Coulaloglou and Tavlarides (1977), Prince and Blanch (1990) and a more recent one

by Lehr *et al.* (2002) to form six different combinations of kernels. The resulted bubble size distributions are compared to achieve a better insight of the prediction mechanisms. Also, the void fraction and interfacial area concentration profiles are compared against the experimental data of Yun *et al.* (1997), Lee *et al.* (2002) and Ozar *et al.* (2013) to ensure the validity of the simulations.

## MATHEMATICAL MODELING

### Two-fluid Model

The ensemble-averaged mass and momentum transport equations for continuous and dispersed phases are modelled using the Eulerian modelling framework. Considering the liquid ( $\alpha^l$ ) as continuous phase and bubbles ( $\alpha^g$ ) as disperse phase, the numerical simulations are presented based on the two-fluid model Eulerian-Eulerian approach.

Continuity equation,

$$\frac{\partial(\rho^k \alpha^k)}{\partial t} + \nabla \cdot (\rho^k \alpha^k \mathbf{u}^k) = \Gamma_{km}(k, m = l, g) \quad (1)$$

Momentum equation,

$$\begin{aligned} \frac{\partial(\rho^k \alpha^k)}{\partial t} + \nabla \cdot (\rho^k \alpha^k \mathbf{u}^k) \\ = -\alpha^k \nabla P + \alpha^k \rho^k g \\ + \nabla \cdot [\alpha^k \mu_g^k (\nabla \mathbf{u}^k + (\nabla \mathbf{u}^k)^T)] \\ + F_{km}(k, m = l, g) \end{aligned} \quad (2)$$

### Bubble Interfacial Forces

According to previous studies, the phase distribution is predominated by the interfacial momentum transfer between two phases. The total interfacial force ( $F_{km}$ ), appearing in equation (2) is formulated based on the appropriate consideration of different interfacial sub-forces acting on each phase. Considering liquid as the primary phase, the total interfacial force is given by the drag, lift, wall lubrication and turbulent dispersion force.

$$F_{lg} = F_{lg}^{drag} + F_{lg}^{lift} + F_{lg}^{wall\ lubrication} + F_{lg}^{turbulent\ dispersion} \quad (3)$$

The mathematical correlations for the interfacial forces are given in Table 1.

Interfacial forces	Correlation
$F_{lg}^{drag}$	$\frac{1}{8} C_D a_{if} \rho^l  u^g - u^l  (u^g - u^l)$
$F_{lg}^{lift}$	$C_L \alpha^g \rho^l (\nabla \times u^l) \times (u^g - u^l)$
$F_{lg}^{wall\ lubrication}$	$-\frac{\alpha^g \rho^l [(u^g - u^l) - ((u^g - u^l) \cdot n_w)]^2}{D_s (C_{w1} + C_{w2} \frac{D_s}{\lambda_w}) n_w}$
$F_{lg}^{turbulent\ dispersion}$	$-C_{TD} \left[ \frac{1}{8} C_D a_{if} \rho^l  u^g - u^l  \right] \frac{\mu_t^g}{\rho^g S c_b} \left( \frac{\nabla \alpha^g}{\alpha^g} - \frac{\nabla \alpha^l}{\alpha^l} \right)$

**Table 1:** Mathematical correlations for interfacial forces

The interfacial mass transfer rate due to condensation in the bulk subcooled liquid in equation (1) can be expressed as:

$$\Gamma_{lg} = \frac{h a_{if} T_{sub}}{h_{fg}} \quad (4)$$

where  $h$  represents the inter-phase heat transfer coefficient.

In equation (2), effective viscosity ( $\mu_e^l$ ) for the continuous liquid phase is the summation of laminar, shear-induced turbulence, and Sato's bubble-induced turbulent viscosities. The shear-induced turbulence is modelled by the Shear Stress Transport (SST) model while Sato's turbulent viscosity model is adopted to consider the bubble-induced turbulence. The expressions for these terms are elaborated in the literature (Deju *et al.* (2013)).

### Population Balance Model

Population balance equations (PBEs) have been applied in many diverse applications which involve particulate systems. The particle (bubble) size distribution is calculated according to the population balance equation that is generally expressed in an integro-differential form:

$$\frac{\partial f(x, \xi, t)}{\partial t} + \nabla \cdot (V(x, \xi, t)f(x, \xi, t)) = S(x, \xi, t) \quad (5)$$

where  $f(x, \xi, t)$  is the particle (bubble) number density distribution per unit mixture and particle (bubble) volume,  $V(x, \xi, t)$  is velocity vector in external space dependent on the external variables  $x$  for a given time  $t$  and the internal space  $\xi$  whose components could be characteristic dimensions such as volume, mass etc. On the right hand side, the term  $S(x, \xi, t)$  contains the particle (bubble) source/sink rates per unit mixture volume due to the particle (bubble) interactions such as coalescence, break-up and phase change.

Homogeneous MUSIG represents the most commonly used technique for solving PBE. The discrete form of the number density equation, expressed in terms of size fraction  $f_i$  of  $M$  bubble size groups, can be written as:

$$\frac{\partial \rho_j^g \alpha_j^g f_i}{\partial t} + \nabla \cdot (u^g \rho_j^g \alpha_j^g f_i) = S_i \quad (6)$$

In the above equation,  $S_i$  represents the net change in the number density distribution due to coalescence and break-up processes. This entails the use of a fixed non-uniform volume distribution along a grid, which allows a range of large sizes to be covered with a small number of bins and yet still offers good resolution. Such discretisation of the population balance equation has been found to allow accurate determination of the desired characteristics of the number density distribution. The interaction term  $S_i = (B_c + B_B + D_c + D_B)$  contains the source rates of  $B_c$ ,  $B_B$ ,  $D_c$  and  $D_B$ , which are the birth rates due to coalescence ( $B_c$ ) and break-up ( $B_B$ ) and the death rates to coalescence ( $D_c$ ) and break-up ( $B_B$ ) of bubbles respectively.

### Coalescence kernels

For coalescence between fluid particles, the coalescence efficiency  $a(M_i, M_j)$  could be calculated as a product of collision frequency,  $h(M_i, M_j)$  and coalescence efficiency,  $\lambda(M_i, M_j)$ .

$$a(M_i, M_j) = h(M_i, M_j)\lambda(M_i, M_j) \quad (7)$$

In the following subsections, the coalescence kernels adopted in this paper are introduced in detail.

### Coulaloglou & Tavlarides (1977)

Coulaloglou and Tavlarides (1977) developed their model based on the consideration of turbulent random motion induced collisions as primary source of bubble coalescence. The collision frequency has been defined as the effective volume swept away by the moving particle per unit time.

$$h(M_i, M_j) = \frac{\pi}{4} (d_i + d_j)^2 (u_{ti}^2 + u_{tj}^2)^{1/2} \quad (8)$$

The turbulent velocity  $u_t$  in the inertial sub-range of isotropic turbulence is given by,

$$u_t = C_1 (\varepsilon d)^{1/3} \quad (9)$$

Then, the collision frequency becomes as,

$$h(M_i, M_j) = C_2 (d_i^2 + d_j^2) (d_i^{2/3} + d_j^{2/3})^{1/2} \varepsilon^{1/3} \quad (10)$$

The value for the constant  $C_2$  has been taken as 1.

As only a fraction of collisions lead to coalescence, it is necessary to incorporate the coalescence efficiency to determine the coalescence rate. They developed their coalescence model based on the film drainage model for deformable particle with immobile surface.

$$\lambda(M_i, M_j) = \exp \left[ -C_{C\&T} \times \frac{\mu_l \rho_l \varepsilon}{\sigma^2} \left( \frac{d_i d_j}{d_i + d_j} \right)^4 \right] \quad (11)$$

Finally the total coalescence rate is calculated from the equation (10) and (11).

$$a(M_i, M_j) = C_2 (d_i + d_j)^2 (d_i^{2/3} + d_j^{2/3})^{1/2} \varepsilon^{1/3} \exp \left[ -C_{C\&T} \times \frac{\mu_l \rho_l \varepsilon}{\sigma^2} \left( \frac{d_i d_j}{d_i + d_j} \right)^4 \right] \quad (12)$$

Based on the experimental data, the coalescence efficiency parameter ( $C_{C\&T}$ ) was selected as  $0.183 \times 10^{10} \text{ cm}^{-2}$ .

### Prince & Blanch (1990)

Turbulent random collision is considered for the bubble coalescence by Prince and Blanch (1990). In their paper, coalescence process in turbulent flows has been described in three steps. Firstly, the bubbles trap small amount of liquid between them. Then the liquid drains out until the liquid film thickness reaches a critical thickness. Finally, the bubbles rupture and coalesce together. Coalescence rate of bubbles has been proposed based on the collision rate of bubbles and the probability at which collision will result in coalescence. The collision frequency calculated similarly as.

$$h(M_i, M_j) = C_3 (d_i + d_j)^2 (d_i^{2/3} + d_j^{2/3})^{1/2} \varepsilon^{1/3} \quad (13)$$

The coalescence efficiency for deformable particle with mobile surfaces has been given by as following.

$$\lambda(M_i, M_j) = \exp \left( -\frac{t_{ij}}{\tau_{ij}} \right) \quad (14)$$

Finally the total coalescence rate by Prince and Blanch (1990) is calculated as following,

$$a(M_i, M_j) = C_3 (d_i + d_j)^2 (d_i^{2/3} + d_j^{2/3})^{1/2} \varepsilon^{1/3} \exp \left( -\frac{t_{ij}}{\tau_{ij}} \right) \quad (15)$$

### Lehr *et al.* (2002)

Lehr *et al.* (2002) proposed the coalescence frequency based on the critical approach velocity model. An experimental investigation has been conducted to determine the criterion of collision between two bubbles

resulting in coalescence or bouncing. They found it depending on the relative approach velocity perpendicular to the surface of contact. They have defined the critical velocity as the maximum velocity of bubbles resulting in coalescence which has no dependency on the size of the bubbles. Collisions will result in coalescence only when the relative approach velocity of bubbles perpendicular to the surface of contact is lower than the critical approach velocity.

The collision frequency function based on this model is as follows.

$$h(M_i, M_j) = \frac{\pi}{4} (d_i + d_j)^2 \min(u', u_{critical}) \exp \left[ - \left( \frac{\alpha_{max}^{1/3}}{\alpha^{1/3}} - 1 \right)^2 \right], \alpha_{max} = 0.6 \quad (16)$$

The characteristic velocity ( $u'$ ) is equivalent to the turbulent eddy velocity with the similar length scale of the bubbles. The smaller eddies would not have sufficient energy to have significant impact on bubbles to collide. On the other hand, larger eddies would end up to transport the bubbles. For the larger eddies, characteristic velocity has been defined as the difference between the rise velocities of the bubbles. This can be expressed as follows,

$$u' = \max \left( \sqrt{2} \varepsilon^{1/3} \sqrt{d_i^{2/3} + d_j^{2/3}}, |\bar{u}_i - \bar{u}_j| \right) \quad (17)$$

Finally the collision frequency can be expressed as,

$$h(M_i, M_j) = C_4 (d_i + d_j)^2 (d_i^{2/3} + d_j^{2/3})^{1/2} \varepsilon^{1/3} \exp \left[ - \left( \frac{\alpha_{max}^{1/3}}{\alpha^{1/3}} - 1 \right)^2 \right], \alpha_{max} = 0.6 \quad (18)$$

And the coalescence efficiency is given by.

$$\lambda(M_i, M_j) = \min \left( \frac{u_{critical}}{u'}, 1 \right) \quad (19)$$

Then the coalescence rate will be calculated as a product of collision frequency and coalescence efficiency.

$$a(M_i, M_j) = C_4 (d_i + d_j)^2 (d_i^{2/3} + d_j^{2/3})^{1/2} \varepsilon^{1/3} \exp \left[ - \left( \frac{\alpha_{max}^{1/3}}{\alpha^{1/3}} - 1 \right)^2 \right] \min \left( \frac{u_{critical}}{u'}, 1 \right) \quad (20)$$

### Breakup kernels

For breakup of fluid particles, the partial breakage frequency  $r(M_i, M_j)$  is a function of total breakage frequency,  $r(M_i)$  and the daughter size distribution,  $\beta(M_i, M_j)$ .

$$\beta(M_i, M_j) = \frac{r(M_i, M_j)}{r(M_i)} \quad (21)$$

### Luo & Svendsen (1996)

Bubble break-up rate by Luo and Svendsen (1996) is based on the assumption of bubble binary break-up under isotropic turbulence situation. Breakup event is determined by the energy level of arriving eddy with smaller or equal length scale compared to the bubble diameter to induce the oscillation. The daughter size

distribution is accounted using a stochastic break-up volume fraction  $f_{BV}$ . The break-up rate in terms of mass can be obtained as:

$$r(M_i, M_j) = 0.923(1 - \alpha_g) n \left( \frac{\varepsilon}{d_j} \right)^{1/3} \int_{\xi_{min}}^1 \frac{(1 + \xi)^2}{\xi^{11/3}} P_b(f_{BV}|d_i, \lambda) d\xi \quad (22)$$

The breakage probability,  $P_b(f_{BV}|d_i, \lambda)$  calculated by using the energy distribution of turbulent eddies. The energy distribution of eddies with size  $\lambda$  is as follows:

$$P_e(e(\lambda)) = \frac{1}{\bar{e}(\lambda)} \exp \left( - \frac{e(\lambda)}{\bar{e}(\lambda)} \right) \quad (23)$$

$\bar{e}(\lambda)$  is the mean kinetic energy of an eddy with size  $\lambda$ . Finally the breakage rate becomes,

$$r(M_i, M_j) = 0.923(1 - \alpha_g) n \left( \frac{\varepsilon}{d_j} \right)^{1/3} \int_{\xi_{min}}^1 \frac{(1 + \xi)^2}{\xi^{11/3}} \exp \left( - \frac{12C_f \sigma}{\beta \rho_f \varepsilon^{2/3} d_i^{5/3} \xi^{11/3}} \right) d\xi \quad (24)$$

From equation (22),  $r(M_i, M_j)$  represents the breakage rate of bubble with mass of  $M_i$  into fraction of  $f_{BV}$  and  $f_{BV} + df_{BV}$  for a continuous  $f_{BV}$  function. The total breakage rate of bubbles can be obtained by integrating the equation (22) over the whole interval of 0 to 1.

Total breakage rate can be expressed as,

$$r(M_i) = \frac{1}{2} \int_0^1 r(M_i, M_j) df_{BV} \quad (25)$$

The advantage of this model is that it provides the partial breakage rate,  $r(M_i, M_j)$  directly. Then the daughter bubble size distribution can be derived by normalizing the partial breakup rate,  $r(M_i, M_j)$  by the total breakup rate,  $r(M_i)$ .

$$\beta(f_{BV}, 1) = \frac{r(M_i, M_j)}{r(M_i)} = \frac{2 \int_{\xi_{min}}^1 \frac{(1 + \xi)^2}{\xi^{11/3}} \exp \left( - \frac{12C_f \sigma}{\beta \rho_f \varepsilon^{2/3} d_i^{5/3} \xi^{11/3}} \right) d\xi}{\int_0^1 \int_{\xi_{min}}^1 \frac{(1 + \xi)^2}{\xi^{11/3}} \exp \left( - \frac{12C_f \sigma}{\beta \rho_f \varepsilon^{2/3} d_i^{5/3} \xi^{11/3}} \right) d\xi df_{BV}} \quad (26)$$

### Wang et al. (2003)

While Luo and Svendsen (1996) only considered the energy constraint, Wang et al. (2003) extended the model by adding the capillary constraint to calculate the breakage. According to this model, the dynamic pressure of the turbulent eddy must be larger than the capillary pressure resulting in minimum breakup fraction. On the other hand, eddy kinetic energy must be larger than the increase of the surface energy resulting in maximum breakup. The advantage of this model is to have no adjustable parameter and provide the daughter size distribution directly by normalizing the partial breakup frequency by the total frequency.

$$r(M_i, M_j) = 0.923(1 - \alpha_d) n \varepsilon^{1/3} \int_{\lambda_{min}}^{d_i} P_b(f_{BV}|d_i, \lambda) \frac{(\lambda + d)^2}{\lambda^{11/3}} d\lambda \quad (27)$$

The total breakup rate can be calculated by,

$$r(M_i) = \int_0^{0.5} r(M_i, M_j) df_{BV} \quad (28)$$

The daughter bubble size distribution is expressed as,

$$\beta(f_{BV}, 1) = \frac{\int_{\lambda_{min}}^{d_i} \frac{(\lambda + d)^2}{\lambda^{11/3}} \int_0^{\infty} \frac{1}{f_{BV,max} - f_{BV,min}} \frac{1}{\bar{e}(\lambda)} d\lambda}{\int_0^1 \int_{\lambda_{min}}^{d_i} \frac{(\lambda + d)^2}{\lambda^{11/3}} \int_0^{\infty} \frac{1}{f_{BV,max} - f_{BV,min}} \frac{1}{\bar{e}(\lambda)} d\lambda \exp\left(-\frac{e(\lambda)}{\bar{e}(\lambda)}\right) de(\lambda) d\lambda} \exp\left(-\frac{e(\lambda)}{\bar{e}(\lambda)}\right) de(\lambda) d\lambda df_{BV} \quad (29)$$

## EXPERIMENTAL DETAILS

In order to assess the vapor distribution in the radial direction for low and medium pressures, three experiments are investigated. Experimental conditions for low pressure (Cases P143) and elevated pressure (Cases P218, P497 and P949) data are presented in Table 2. These cases cover a range of different flow conditions including pressure, inlet liquid velocity, wall heat flux and inlet subcooling temperature that play important roles on vapor phase distribution and wall heat flux partitioning. The authors tried to illustrate the underlying physics through the results obtained by simulations. For each case, simulation results are validated against available data of these experiments. To help the readers understand the experimental conditions investigated in this paper, the details of experiments are given as follows. For more details refer to the references cited below.

Low pressure experiment performed by Yun *et al.* (1997) and Lee *et al.* (2002) consisted of a vertical concentric annulus with an inner diameter of 37.5 mm for the outer wall, and outer diameter of 19 mm for the inner heating rod as the test section; the working fluid was demineralised water. The heated section was 1.67 m long and entire rod was heated by a 54 kW DC power supply. Radial measurements of phasic parameters were done at 1.61 m downstream of the start of the heated section. A two-conductivity probe method was used to measure local gas phase parameters such as local void fraction, bubble frequency and bubble velocity. The bubble Sauter mean diameters (assuming spherical bubbles) were determined through the interfacial area concentration (IAC), calculated using the measured bubble velocity spectrum and bubble frequency. The uncertainties in the measurement of local void fraction, velocity, volumetric flow rate, temperature, heat flux and pressure are estimated to be within  $\pm 3.0\%$ ,  $\pm 3.3\%$ ,  $\pm 1.9\%$ ,  $\pm 0.2^\circ\text{C}$ ,  $\pm 1.7\%$  and  $\pm 0.0005\text{ MPa}$ , respectively.

Ozar *et al.* (2013) performed medium pressure experiments where a vertical concentric annulus was employed. The outer wall's inner diameter was 38.1 mm, and the inner heating rod had 19.1 mm outer diameter. The annulus was designed between the pipes and the cartridge heater. The heated section was 2.845 m long which was followed by a 1.632 m long unheated section. The heater could produce a maximum heat flux of  $260\text{ kW/m}^2$ . The measurements presented in this paper, were performed at 2.05 m downstream of the start of the heated section. The uncertainties in the measurement of local void fraction (done through a 4-sensor conductivity probe), gas velocity, flow rate, temperature and pressure are estimated

to be less than 10%, less than 10%, within  $\pm 0.75\%$ ,  $\pm 2.2^\circ\text{C}$  and less than  $\pm 0.2\%$ , respectively.

Case	P <sub>inlet</sub> (kPa)	T <sub>inlet</sub> (°C)	T <sub>sub@inlet</sub> (°C)	Q <sub>w</sub> (kW/m <sup>2</sup> )	G (kg/m <sup>2</sup> s)
P143	143	92.1	17.9	251.5	1059.2
P218	218	110.3	12.7	237.9	1843.8
P497	497	136.7	14.8	190.9	942.3
P949	949	167.6	10.0	208.5	964.4

**Table 2:** Experimental conditions for different Cases

## RESULTS AND DISCUSSION

In order to discretise the conservation equations of mass, momentum and energy, the finite volume method is employed. Mentioned equations for each phase along with 15 extra set of transport equations for capturing coalescence, break-up and condensation of the bubbles for the MUSIG boiling model are solved. Since a uniform wall heat flux is applied, only a 60° section of the annulus is modeled as the computational domain for all the cases. Grid independence is inspected for 45, 90, 180, 240 and 300 cells along the vertical direction, and 5, 10, 20 and 30 cell in the radial direction; the mean velocity profiles of liquid and gas, and the volume fraction distribution did not change significantly by further grid refinement of 180 cells in the vertical direction and 10 cells in the radial direction. The proposed mechanistic approach along with some of the existing empirical correlations are compared against experimental data of Yun *et al.* (1997) and Lee *et al.* (2002) for Case P143 and Ozar *et al.* (2013) for Cases P218–P949. The proposed mechanistic model consists of fractal wall heat flux partitioning model. For the break-up kernels, two widely adopted models with different predictions for daughter size distribution (DSD) proposed by Luo and Svendsen (1996) and Wang *et al.* (2003) are selected. These break-up kernels are then coupled with three different coalescence kernels by Coualoglou and Tavlarides (1977), Prince and Blanch (1993) and a more recent one by Lehr *et al.* (2002) to form six different combinations of kernels. The list of these combinations of kernels are given in Table 3.

No.	Coalescence Kernel	Break-up Kernel
1	Prince and Blanch (1993)	Luo and Svendsen (1996)
2	Prince and Blanch (1993)	Wang <i>et al.</i> (2003)
3	Coualoglou and Tavlarides (1977)	Luo and Svendsen (1996)
4	Coualoglou and Tavlarides (1977)	Wang <i>et al.</i> (2003)
5	Lehr <i>et al.</i> (2002)	Luo and Svendsen (1996)
6	Lehr <i>et al.</i> (2002)	Wang <i>et al.</i> (2003)

**Table 3:** List of different kernel combinations

### Mean Sauter Bubble Diameter Profiles

In Fig. 1, the predicted mean Sauter bubble diameter profiles in the radial direction for six aforementioned kernels are presented against the experimental data of Yun *et al.* (1997) and Lee *et al.* (2002) for Case P143 and experiments of Ozar *et al.* (2013) for Cases P218–P949.

The coalescence kernels do not seem to have a significant contribution in the prediction of the bubble size. Among the coalescence kernels, Coualoglou and Tavlarides tend to predict a higher rate of bubbles merging together and Lehr *et al.* predict a lower rate.

All the kernels predict the bubble size closely near the heated wall region; however, away from the heated wall in the bulk liquid region the kernels 2, 4, 6 with similar

break-up kernel of Wang et al. predict differently to the kernels 1, 3, 5 with break-up kernel of Luo and Svendsen. For the lower pressure cases (Cases P143-P497), the break-up kernel of Wang et al. tends to over-predict the bubble size in the subcooled region. This means that the rate of break-up for this model is lower than that of Luo and Svendsen. However, for the Case P949 where two-

group bubble is present, the Wang et al. kernel predicts better. Nonetheless, the only parameter influential on the bubble size is not the break-up kernel. The condensation in the subcooled region as well as the influence of different bubble shapes (rather than spherical) should be also investigated.

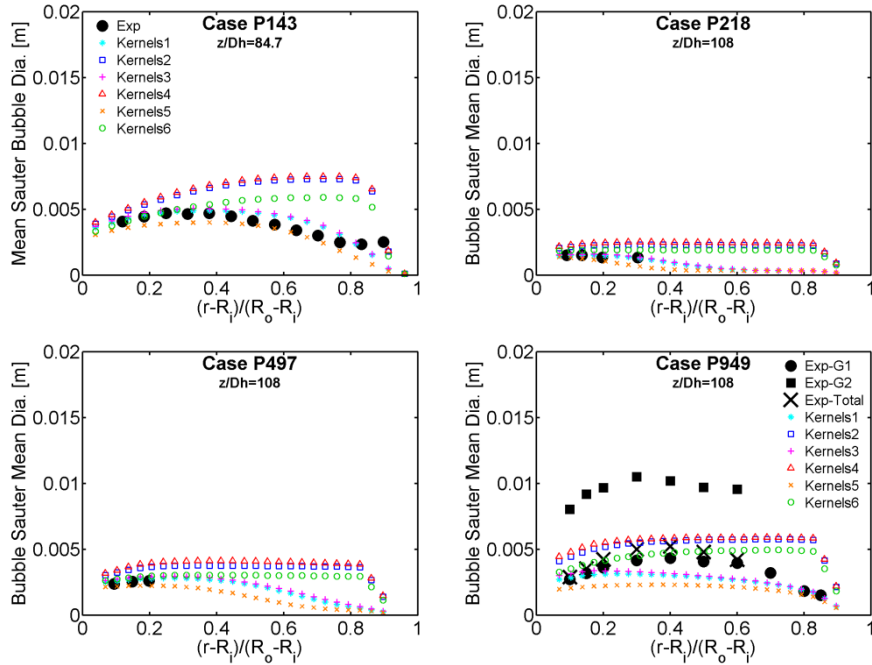


**Figure 1:** Predicted radial distribution of bubble Sauter mean diameter for Cases P143-P949.

### Void Fraction Profiles

Fig. 2 presents the predicted void fraction profiles in the radial direction for six aforementioned kernels against the experimental data of Yun *et al.* (1997) and Lee *et al.* (2002) for Case P143 and experiments of Ozar *et al.* (2013) for Cases P218-P949.

For all cases, the trend of void fraction distribution is captured accurately. A higher void fraction near the heated wall is due to the vapor generation at the surface of the heated wall. Later, when the bubbles are exposed to the subcooled liquid, they get condensed and the void fraction is reduced. However, an over-prediction of void fraction near the heated wall is observed. All six kernels predict closely for lower pressure cases (Cases P143-P497); yet the kernels 2, 4 and 6 predict more accurately for the elevated pressure case (Case P949). In this Case, two groups of bubbles are present which leads to higher void fractions compared to other Cases. The lower break-up rate that is predicted by Wang et al. helps to have more accurate results in such cases.

### Interfacial Area Concentration Profiles

The Interfacial Area Concentration (IAC) profiles in the radial direction for six kernels are depicted against the experimental data of Yun *et al.* (1997) and Lee *et al.*

(2002) for Case P143 and experiments of Ozar *et al.* (2013) for Cases P218-P949 in Fig. 3. The influence of different coalescence kernels is not significant in the prediction of IAC profile for different cases.

The Kernels 1, 3, 5 with Luo and Svendsen's break-up model tend to over-predict the IAC at the near heated wall region; while, the Kernels 2, 4, 6 with Wang et al.'s break-up model predict the IAC in the vicinity of the heated wall better. The over-prediction of IAC in Luo and Svendsen's model in conjunction with the over-prediction of void fraction (as was observed in Fig. 2, especially for the Case P-497), leads to a better prediction of the bubble size (as was observed in Fig. 1) compared to the Kernels with Wang et al.'s break-up model.

Similar to other radial profiles, the Wang *et al.* (2003)'s model performs better in the prediction of IAC profile at the elevated pressure case (Case P949). This could be attributed to the formulation of the Wang et al.'s model: as mentioned in the mathematical modelling section, the bubbles will breakup only when the dynamic pressure of the approaching turbulent eddy is higher than the capillary pressure of bubbles. Therefore, the influence of pressure is considered in this model which leads to better prediction of all radial profiles of mean Sauter bubble diameter, void fraction, and IAC for the Case P949.

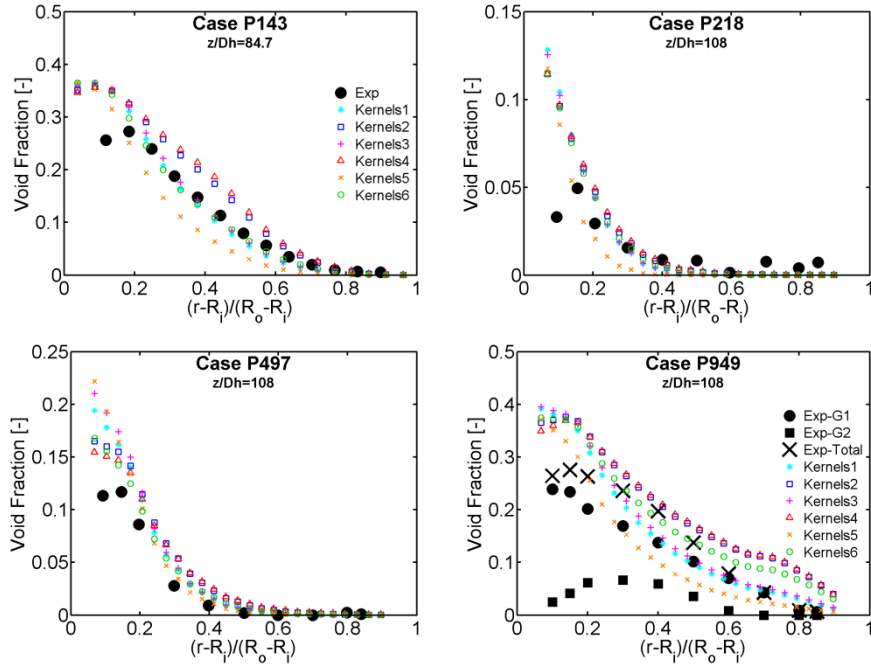


Figure 2: Predicted radial distribution of void fraction for Cases P143-P949.

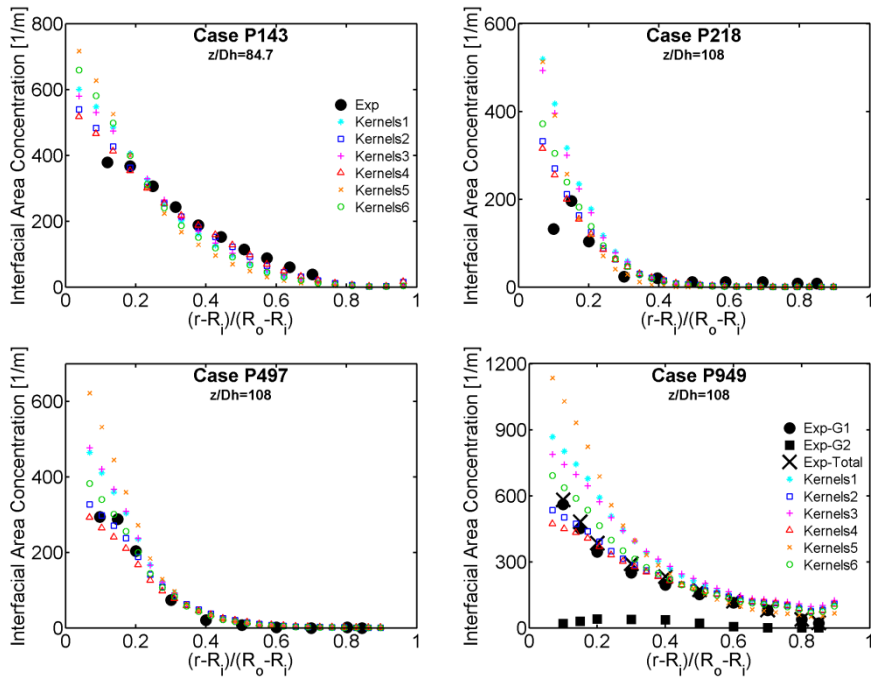


Figure 3: Predicted radial distribution of Interfacial area concentration for Cases P143-P949.

## CONCLUSION

In this paper, the performance of different coalescence and breakage kernels is investigated through numerical simulations. The influence of these kernels on the bubble size and local hydrodynamic variables in the subcooled boiling flow in vertical pipes is captured. The numerical predictions are validated against the experimental data of Yun et al. (1997) and Lee et al. (2002) for Case P143 and experiments of Ozar et al. (2013) for Cases P218-P949. Overall, the bubble size, void fraction and IAC profiles' trends are reasonably captured by these kernels.

Interestingly, the influence of different coalescence kernels investigated in this study is found to be insignificant; however, more profound effects are observed by altering the break-up kernels. The model by Luo and Svendsen seems to predict a higher rate of break-up, resulting in a better prediction of bubble size and void fraction for lower pressure cases. Nonetheless, the consideration of capillary pressure in the Wang et al.'s break-up model resulted in better predictions for the elevated pressure case.

## ACKNOWLEDGEMENT

The financial support provided by the Australian Research Council, Australia (ARC project ID DP130100819) is gratefully acknowledged.

## REFERENCES

- COULALOGLOU, C. and L. TAVLARIDES (1977). "Description of interaction processes in agitated liquid-liquid dispersions." *Chemical Engineering Science*, **32**(11): 1289-1297.
- DEJU, L., et al. (2015). "Comparative Analysis of Coalescence and Breakage Kernels in Vertical Gas-Liquid Flow." *Canadian Journal of Chemical Engineering*, **93**(7): 1295-1310.
- DEJU, L., et al. (2013). "Capturing coalescence and break-up processes in vertical gas-liquid flows: Assessment of population balance methods." *Applied Mathematical Modelling*, **37**(18-19): 8557-8577.
- LEE, T. H., et al. (2002). "Local flow characteristics of subcooled boiling flow of water in a vertical concentric annulus." *International Journal of Multiphase Flow*, **28**(8): 1351-1368.
- LEHR, F., et al. (2002). "Bubble-size distributions and flow fields in bubble columns." *Aiche Journal*, **48**(11): 2426-2443.
- LIAO, Y. and D. LUCAS (2009). "A literature review of theoretical models for drop and bubble breakup in turbulent dispersions." *Chemical Engineering Science*, **64**(15): 3389-3406.
- LIAO, Y. X. and D. LUCAS (2010). "A literature review on mechanisms and models for the coalescence process of fluid particles." *Chemical Engineering Science*, **65**(10): 2851-2864.
- LUO, H. and H. F. SVENDSEN (1996). "Theoretical model for drop and bubble breakup in turbulent dispersions." *AIChE Journal*, **42**(5): 1225-1233.
- OZAR, B., et al. (2013). "Interfacial area transport of vertical upward steam-water two-phase flow in an annular channel at elevated pressures." *International Journal of Heat and Mass Transfer*, **57**(2): 504-518.
- PRINCE, M. J. and H. W. BLANCH (1990). "Bubble coalescence and break-up in air-sparged bubble columns." *AIChE Journal*, **36**(10): 1485-1499.
- WANG, T., et al. (2003). "A novel theoretical breakup kernel function for bubbles/droplets in a turbulent flow." *Chemical Engineering Science*, **58**(20): 4629-4637.
- YEOH, G. H., et al. (2014). "Modeling subcooled flow boiling in vertical channels at low pressures – Part 2: Evaluation of mechanistic approach." *International Journal of Heat and Mass Transfer*, **75**(0): 754-768.
- YUN, B. J., et al. (1997). "Measurements of local two-phase flow parameters in a boiling flow channel." *Proceedings of the OECD/CSNI specialist meeting on advanced instrumentation and measurement techniques*.